DEMONSTRATION AT VLISSINGEN

Written by Wikke Witteveen, Raf Meskens, Giani Ramos, Gerrit Van Geffen, Ruben Van Horebeke, and Geert Potters – Antwerp Maritime Academy

The demonstrator

Location

Output 5 compares the conditions and corrosion rates of different port environments. We chose these locations to obtain a wide variety of different conditions:

- The south coast of England (Shoreham, Newhaven) which are in direct contact with the Atlantic Ocean.
- The port of Ostend, close to the North Sea.
- The port of Den Helder in the North of the Dutch province of Noord-Holland.
- The marina of Zelzate, along the canal of Ghent-Terneuzen, which is situated much more inland, and offers brackish water.
- The port of Vlissingen, at the bank of the Westerschelde (leading directly into the North Sea).

The port area of North Sea Port is an area that extends from Ghent to the outer harbour in Vlissingen. The port area has a very large diversity of wet infrastructure, also known as assets. This includes the berths, waterways, mooring buoys, *jetties,* and quay walls. These quay walls extend over 55.6 km. Because the ports in Vlissingen are strongly influenced by the tides and the saltier seawater, this has a major impact on the degradation of the water-related infrastructure. Moreover, it has a direct influence on the maintenance and management of the various assets.

North Sea Port offered us the use of the Calamiteitensteiger at the Sloeweg in Vlissingen.

Two platforms were set up at this location:

- One of these locations, Vlissingen 1 (VL1; Figure 1 top), was attached to a floating jetty, guaranteeing a constant depth of 1 metre. This design ensured that the rack always remained at a stable depth below the surface of the water. The floating jetty provided a platform to which the rack could be attached, maintaining a fixed depth regardless of variations in water level due to tidal movement. This provided a stable environment for the placed materials and facilitated the comparability of measurement results over time. Ensuring the fixed depth of 1 meter made it possible to take accurate and consistent measurements, which was essential for assessing the impact of the environmental factors on the materials exposed to the rack.
- The second platform, Vlissingen 2 (VL2; Figure 1 bottom), was located on the quay to provide slightly different environmental conditions for conducting the study. Here, the rack was attached to a construction against the quay wall, which resulted in variable water depths because of the tide. The height of the quay wall is 14 metres, and the lowest astronomical tide (LAT) is at a height of 6.44 meters above the bottom. The coupons were suspended in such a way that they were always submerged at least 1 meter.

The lowest observed water level in Vlissingen during the period of 2022-2023 was about 0.20 metres, implying that there was always at least 6.64 meters of water present. Therefore, the coupons were suspended at a height of 5.64 meters above the floor (Figure 2). This position was achieved by creating a distance of 7.36 meters between the suspension point and the

racks themselves. The maximum tide during the same period was about 5.30 meters, resulting in a total water height of 11.74 meters. This kept the coupons constantly submerged at a depth that varied between 1 meter and 6.1 metres.

Figure 1. The platforms in Vlissingen.
Top: Vlssingen 1; bottom: Vlissingen 2.

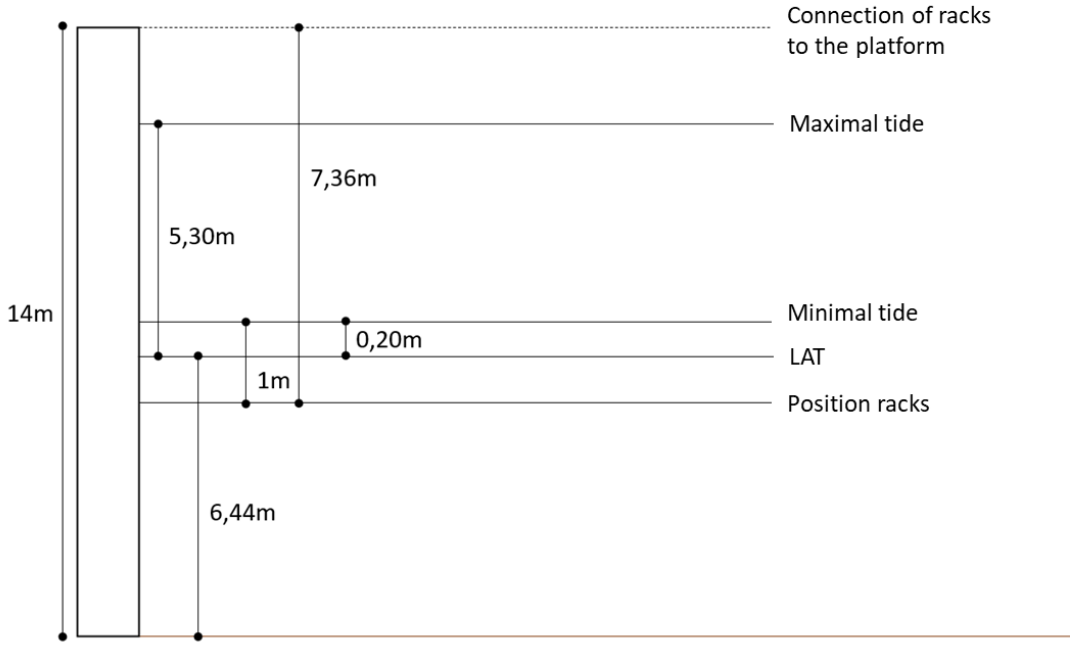

Figure 2.Schematic overview of the depth profile at VL2

Sensor equipment

Both an environmental sensor (Scuba90) and a corrosion sensor (C-Cube) were used. By means of a specially designed distribution box, which was developed for the SOCORRO project, the uploading of data was optimized (Figure 3).

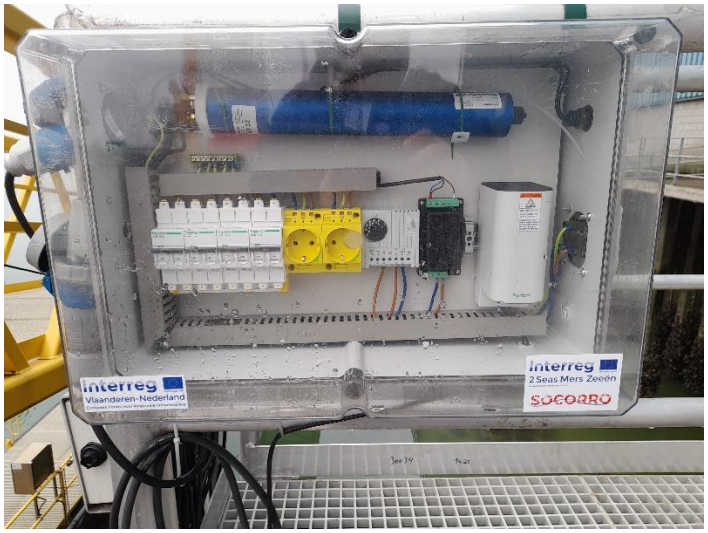

Figure 3. Sensor box at Vlissingen 2.

A **Scuba90 sensor**, manufactured by Royal Eijkelkamp Soil & Water B.V., was used to measure the environmental parameters. (Giesbeek, The Netherlands). In the context of the SOCORRO project, only Scuba sensors were used, which measure specific environmental parameters that influence the corrosion rate. The measured physiochemical factors include temperature, pH, specific conductivity 25°C, salinity, dissolved oxygen, dry matter content, redox potential and chlorine content.

The Scuba90 sensor is 450mm in length and 90mm in diameter. The operating temperature varies within a range of -50°C to +50°C. The maximum operational depth of the sensor is 200 m, while the ion-selective electrode (ISE) can reach a maximum depth of 15 m. The sensor is supplied with a 12 V power supply and has a memory for 1,000,000 measurements (Royal Eijkelkamp, n.d.).

It is a multi-sensor probe equipped with several sensors capable of determining eight parameters (Royal Eijkelkamp, 2022).

- The **temperature** (Figure 4, 1) was measured by means of a thermistor whose resistance changes with temperature. Thermistors are very stable over time and therefore do not require calibration.
- **Dissolved oxygen** was measured using an optical sensor (Figure 4, 2). This sensor consists of a blue light source, a detection surface, and a red-light receiver. When the detection surface is exposed to seawater, a reaction occurs between the oxygen in the seawater and the detection surface. The measurement principle is based on the phenomenon of fluorescence, where the detection surface absorbs light of a specific wavelength and then emits light of a different wavelength. In this case, the surface absorbs blue light and emits red light. During a measurement cycle, the blue light is turned on for a short time, after which the red-light receiver measures the time it takes for the fluorescence to extinguish. This length of time is proportional to the amount of dissolved oxygen in the seawater. It is important to emphasize that the presence of an oxygen active coating on the optical sensor can lead to inaccurate measurements. This is comparable to situations in which photosynthetic algae create a specific microenvironment of oxygen.
- The **specific conductivity of water** is determined by a four-electrode method. The sensor (Figure 4, 3) is equipped with two sets of graphite electrodes carefully positioned for stable measurement. A constant voltage is applied to one pair of electrodes and the current required to maintain this voltage is measured. The current strength increases as the conductivity of the water increases. The Scuba usually displayed specific conductivity, which is standardized to 25°C, representing the conductivity of the water as if the water had been heated or cooled to exactly 25°C. Conductivity can be expressed in different units, such as total dissolved solids (TDS) and salinity, expressed in Practical Salinity Unit (PSU). The values of either parameter were always derived from the specific conductivity.
- The **acidity (pH)** was determined by means of a pH glass electrode (Figure 4, 4). As a result of the ion exchange between the water and the pH glass membrane, a charge separation occurs across the glass. This charge separation creates a voltage difference that can be measured and corresponds to the pH value of the solution.

- The **redox potential** is measured using an oxidation-reduction potential (ORP) sensor (Figure 4, 5). This sensor is located next to the pH sensor and can be noticed as a gray dot of 1 mm diameter. The redox potential is determined by measuring the voltage drop between the platinum membrane of the ORP electrode and the reference electrode. Because platinum does not react with the ions in the water, the redox potential can be derived from this voltage drop.
- An extra fluorimeter (Figure 4, 6) can be used to measure the chlorophyll concentration in the water. This is a measure of the presence of microalgae and therefore an indicator of the biological activity of the marine ecosystem.
- A reference electrode (supporting the other electrode measurements; (Figure 4, 7) and a chloride sensor (Figure 4, 8) complete the setup.

The Scuba probe furthermore comes with two different attachments that serve to protect the sensors. These attachments can be securely attached to the sensors using threads. A sealed capsule is available to store the probe. Since the sensors must be stored in a humid environment, the sealed capsule is partially filled with water before being attached to the probe.

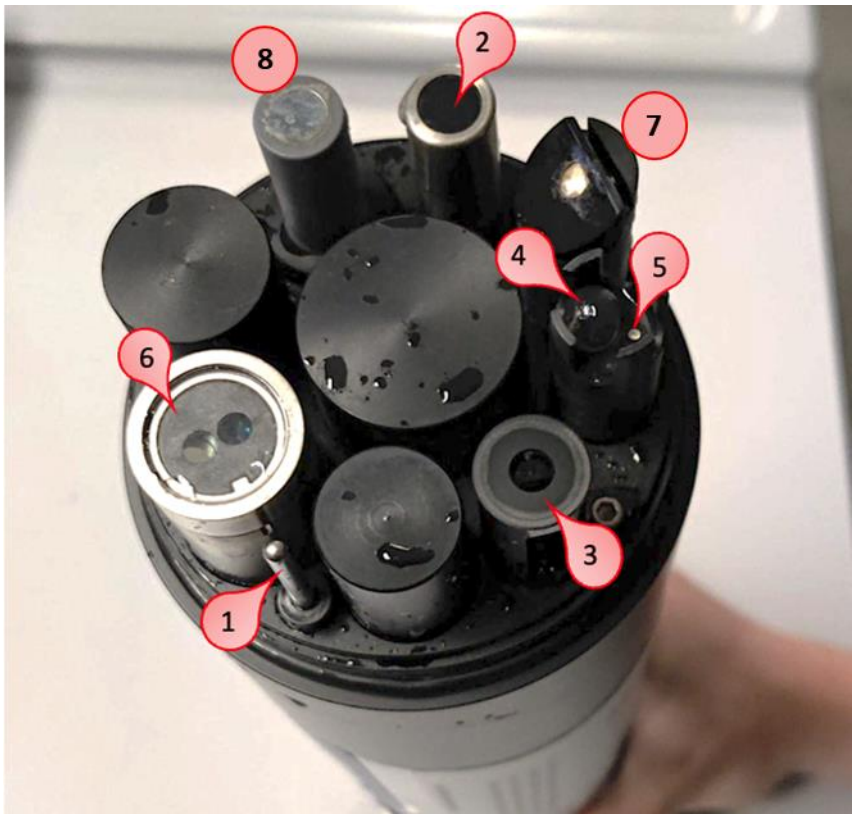

Figure 4. Different sensors of the Scuba Probe.
1: temperature sensor, 2: optical sensor (dissolved oxygen), 3: conductivity sensor, 4: pH glass, 5: ORP sensor, 6: fluorometer for chlorophyll determination; 7. reference electrode; 8. chloride sensor.

An open capsule (Figure 5) is used when the probe is deployed. This capsule contains a weight to sink the Scuba Probe. The openings in the capsule serve on the one hand for the efficient passage of water and on the other hand for the protection of the sensors. The capsule is fitted

with a copper mesh, which acts as a biofouling-resistant barrier. The copper mesh exhibits a controlled solubility, slowly degrading and releasing copper ions. These copper ions cover the surfaces of the sensors and act effectively against the growth of biological organisms.

The Scuba is connected to a 4G modem that uploads the data to the Telecontrolnet platform. Telecontrolnet is a platform where all data from the Scuba sensors come together. Here specific filters were applied to select only the sensors and parameters relevant for this project. Subsequently, a dataset was exported in the form of an Excel file. This Excel file was converted to a CSV file so that it could be uploaded in the bespoke R script for the correlation analysis.

Figure 5. Open capsule for a Scuba probe

Calibration of the environmental sensors

When the secondary Scuba's readings differ from the in-water Scuba's readings, it was replaced or calibrated. The calibration procedure involves instructing the Scuba with the values it should indicate in a specific calibration situation, where the correct parameter value is known (Table 1). This practically implies the use of a liquid with a known value, which is indicated to the Scuba during immersion in this liquid.

Table 1. Calibration of the different sensors on the Scuba 90

Sensor	Calibration method	Calibration points
Temperature	No calibration needed	Not applicable
pH	Two-/three-points	pH 4, pH 7, pH 10
ORP	1 point	ORP standard 200 mV

Conductivity	1 point	CD standard, 0.5 M, 58670 µS (brackish – salt water) CD standard, 0.1 M, 12856 µS (brackish water) CD standard, 0.01 Molar, 1412 µS (freshwater) CD standard, 0.001 Molar, 147 µS (fresh/glacial water)
Dissolved oxygen	1 point	100% saturated distilled water (shaken heavily to saturate water with O_2)

Corrosion probes

For the SOCORRO project, a specific corrosion measurement system has been developed which measures corrosion of three different steel grades (S355, 316L and S235) and a micro-electrochemical cell that measures the rate of corrosion. These measurements are performed every 4 hours.

The working and reference electrodes are housed in a plastic housing filled with epoxy adhesive for protection against sea water. The LP sensor from CCube (Delft, the Netherlands) has dimensions of 150 mm (length) x 60 mm (height) x 50 mm (width).

The sensor is connected to a separate CCube control box located in an easily accessible position. A potentiostat and a data logger are installed in the control cabinet. In addition, the control box contains a mobile antenna that transmits the measured data to the CCube network. The company collects all sensor data and sends it to an online database that is accessible to all researchers of the SOCORRO project.

Sensor box

A sealed electrical distribution box was designed and built within the SOCORRO partnership to power the sensors and support the Scuba while uploading data. To this end, the distribution box is equipped with an internal heating element (Figure 6, 2) to maintain a constant temperature of approximately 15-20 degrees Celsius. This heating element is connected to a thermostat (Figure 6, 3) that controls the activation of the element when the temperature falls below the desired value and switches it off when the maximum temperature is reached. To prevent short circuits and electrical damage to the equipment, the entire distribution box is fitted with fuses (Figure 6, 4). In addition, two CEE 16A plugs (Figure 6, 5) are provided to connect a laptop or other electronic devices on site if necessary.

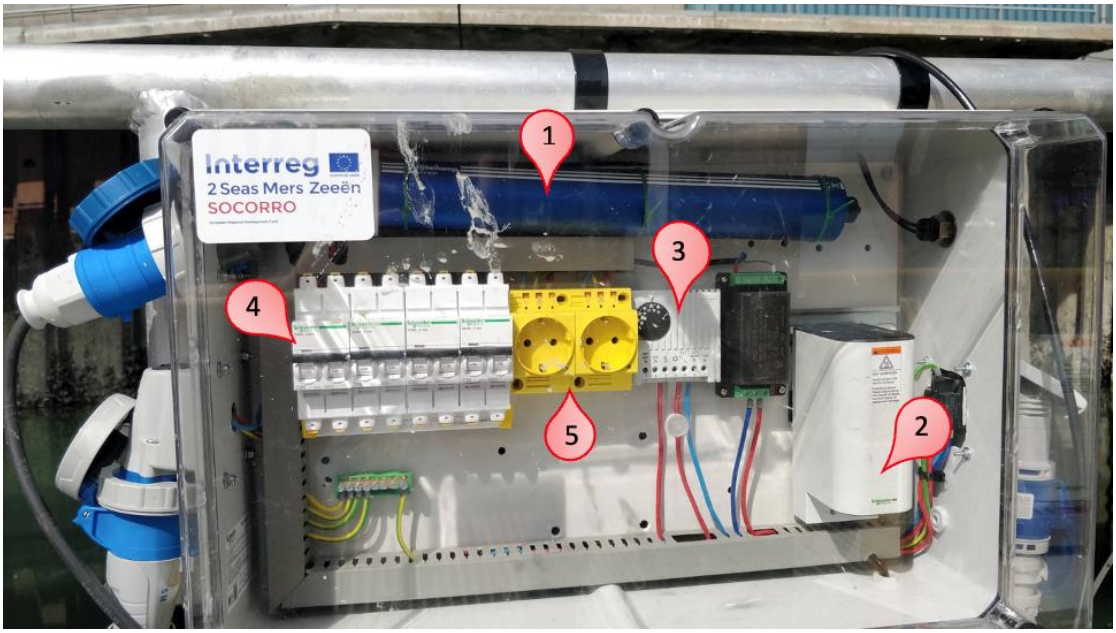

Figure 6. Electrical distribution box for sensors.
1: 4G modem, 2: internal heating, 3: thermostat, 4: circuit breakers, 5: sockets

Data upload

For this purpose, a 4G modem (Figure 6, 1), namely the GDT-S Prime Plus, is integrated in the system (Figure 46). This allowed the data generated by the Scuba sensors to be initially stored and then forwarded to the GDT server at time intervals set by the user. Via this server, users not only had the possibility to view the data via the internet, but also to adjust the settings of the modem and sensors. This could be done via the Eijkelkamp web portal.

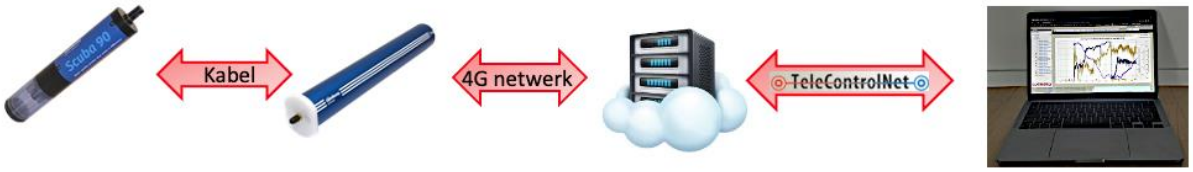

Figure 7. Overview of how data flows from sensor to web portal

Sensor maintenance

To ensure the accuracy of the measurements, it was essential to carry out a thorough maintenance of the sensors. At each visit to the rigs, the sensors were removed from the water and subjected to a thorough visual inspection. It was frequently found that the sensors suffered from biological fouling, which required careful and thorough cleaning. The cleaning process had to be carried out with extreme care to avoid possible damage to the sensors. It was crucial to clean specifically around the sensors and to avoid direct contact with the sensors. For the CCube corrosion probe, it was extremely important to have absolutely no contact with the LP

sensors, as this would disturb the corrosion layers already present on the sensor, which could affect the measurements.

For the maintenance of the Scuba, the initial concern is the external condition of the device. In particular, the copper protective cover, intended to limit biological growth on the sensors, may need to be replaced. Then the Scuba's current readings were analysed using a secondary Scuba. A bucket was used to carefully collect a sample of water from the immediate vicinity of the setup, at a depth of about 1 meter. The bucket should be handled with care to minimize unwanted oxygen entry into the water. The Scuba was placed in the bucket, at approximately 10 cm from the bottom, and then connected to a laptop computer running the Scuba Control Software. The direct measurement values could be observed via this software. After a certain period of time, the values stabilized. The software provided the option to copy a data series.

This data set was then compared to the data received from the Scubas in the water, allowing to calibrate or replace the Scuba to be determined. After the calibration procedure, the secondary Scuba was thoroughly rinsed with distilled water to remove any contaminants, and it was then safely stored, fitted with its protective cap, to maintain the integrity of the device.

Baseline measurements of environmental parameters

It is to be expected that there are considerable similarities between the results of both setups in Vlissingen, given that the sensors were located at a short distance from each other. Any small differences in the results could possibly be attributed to the removal of irregular data points around the end of January in VL1. For this reason, when analysing the results, the results of VL2 will always be considered first. The results analysed here run from August 2022 until April 2023.

Surface temperatures show a pattern beginning in August, rising slightly and then falling gradually from about 23°C to an average swing of around 7°C from December to April (Figure 8). This variability can be explained by seasonal changes. On the one hand, the average air temperature of the area decreases from August, which logically leads to the cooling of the water. On the other hand, the decrease in solar radiation from September also has an impact. Climate statistics (Klimaatinfo.nl and KNMI) show that the average air temperature for Vlissingen decreases from about 21.1°C in August to about 4.9°C in December. Similarly, the UV index shows a decline over this period, according to climate statistics, ranging from UV 3-6 to UV 0-3.

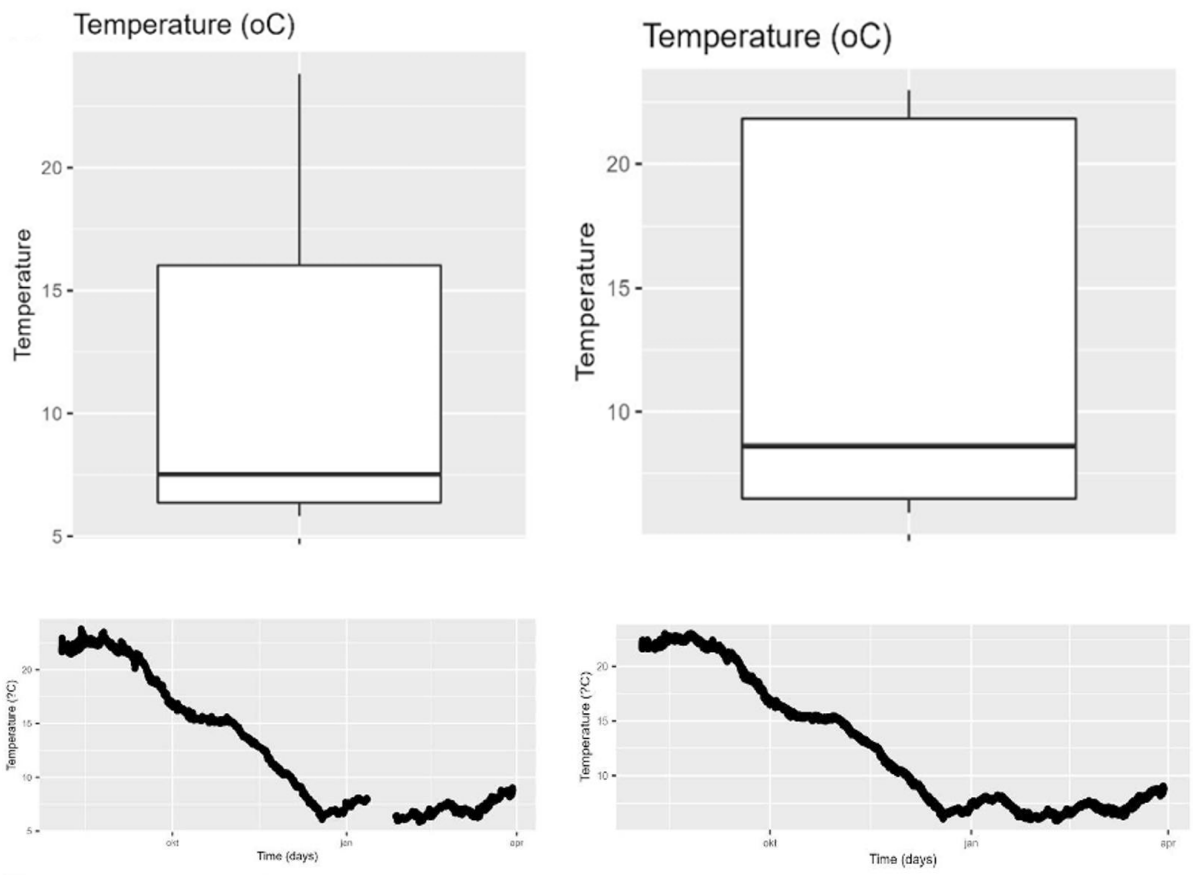

Figure 8. Temperature development of the water in the port of Vlissingen Left: VL1; right: VL2.

The box plot shows that the observations of higher temperatures show more dispersion, while the observations of lower temperatures remain relatively constant. The lower half of the observations are in a narrow range of 6-8°C with little variation, while the upper half of the observations are above this range and show a wider spread. This spread can be attributed to the prolonged cooling of the seawater. On the other hand, the small spread of the lower temperatures may be due to the temperature remaining stable during the winter months.

The time course of the **dissolved oxygen content** (Figure 9) actually shows an inverse relationship with that of the temperature, which makes sense given their close relationship. From August to September there is a slight decrease from 8 to 5 mg/L, followed by a gradual increase to 10 mg/L in February (Figure 68). The measurements end with a slight downward trend in April.

For the dissolved oxygen content in VL2, the median appears to be around 8.5 mg/L. A larger spread can be observed in the observations below 8.5 mg/L than in the observations above 8.5 mg/L. In the case of VL1, the median appears to be slightly higher, around 9.5 mg/L. This will mainly be due to the deletion of several weeks of data in the month of January. The distribution of observations shows a similar pattern, again with a greater spread below the

median than above it. These observations can be explained by the prolonged cooling of the seawater, with the dissolved oxygen content increasing during this period. Since the temperature remained consistently low later in the winter months, the dissolved oxygen content remained stable and high resulting in a much narrower spread of values.

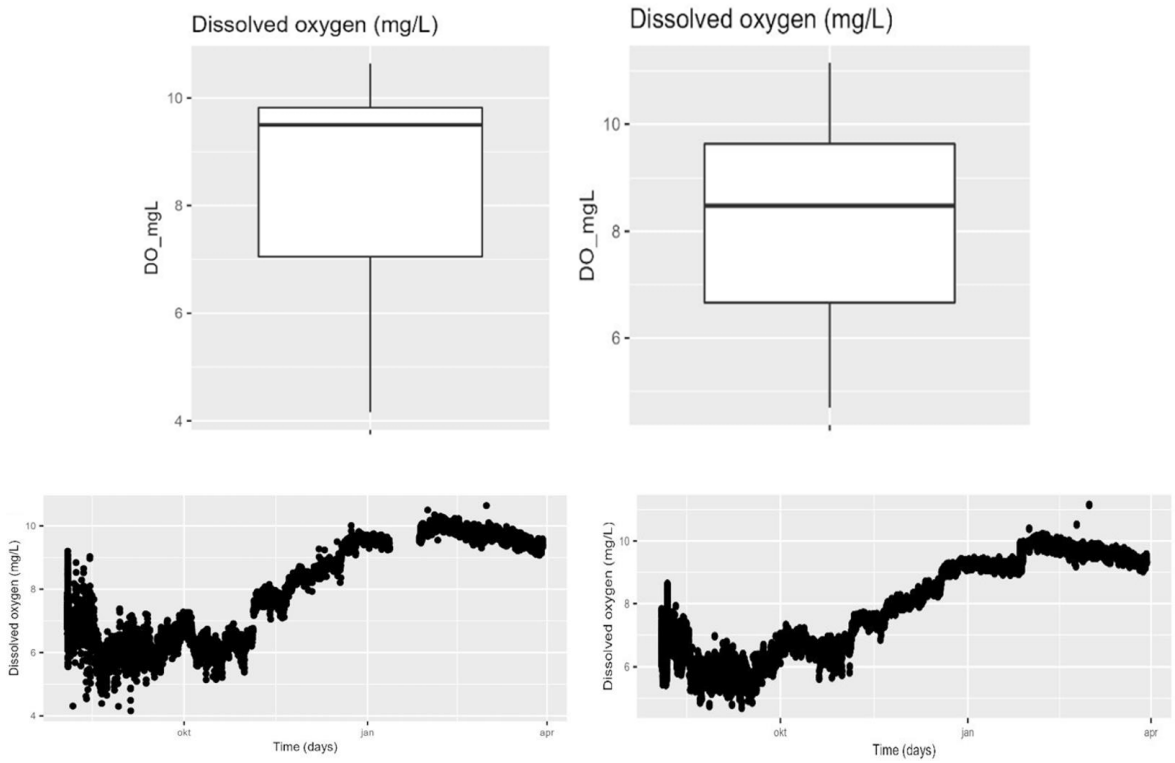

Figure 9. Dissolved oxygen content of the water in the port of Vlissingen
Left: VL1; right: VL2.

In addition to the correlations with other measured parameters, which will be discussed later, the literature also describes relationships between the dissolved oxygen content and the movement and turbulence in the water. For example, currents and waves can help to introduce oxygen into the water through aeration and mixing of air with water (US EPA, 2015). In addition, weather conditions such as rainfall can influence the dissolved oxygen content (US EPA, 2015). Both time series also show that there are some outliers with values around 11 mg/L.

Certain patterns can be observed for **conductivity and salinity of the water**. In the first months of the measurements, the conductivity remains quite stable at around 45 mS/cm (29.5 PSU) for both setups (Figure 10).

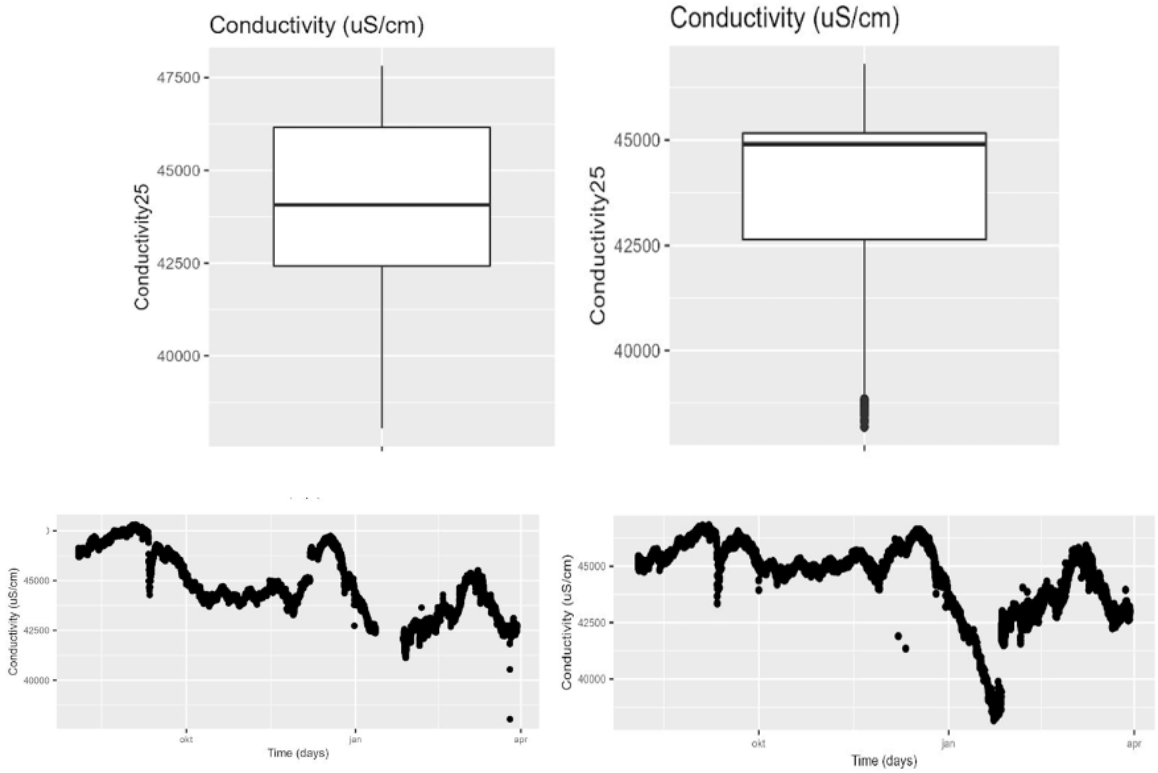

Figure 10. Conductivity (standardised at 25°C) of the water in the port of Vlissingen. Left: VL1; right: VL2.

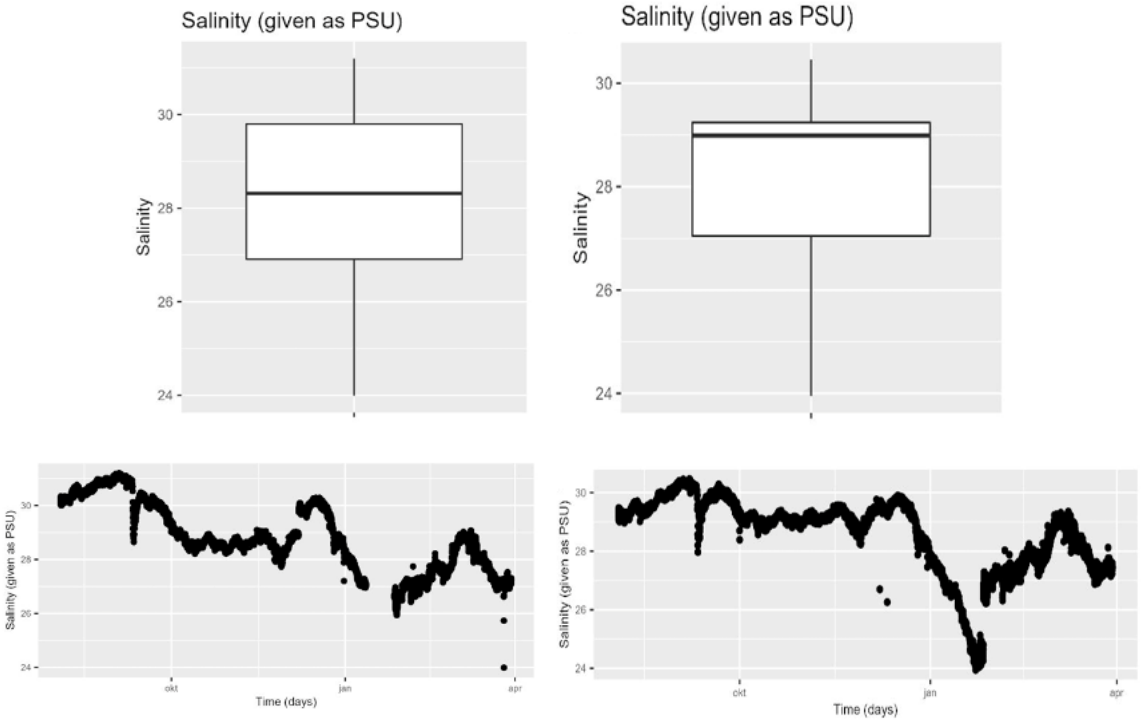

Figure 11. Salinity of the water in the port of Vlissingen.
Left: VL1; right: VL2.

Noteworthy is an irregular falling peak that occurs around the beginning of September. This spike can probably be attributed to the removal of the Scuba on September 12 when placing the racks of coupons. However, a downward trend is visible from mid-December, with conductivity decreasing to about 38 mS/cm in February for VL2. Subsequently, for both setups, there is a gradual increase until early March, with the conductivity increasing again to approximately 45 mS/cm, followed by a further decrease to approximately 42.5 mS/cm.

The VL2 box plot reveals that 50% of the conductivity observations are below 45 mS/cm (29 PSU salinity), though this part accounts for the greatest variation in observations can be found below this median. For VL1, the conductivity appears to follow a more normal distribution around 44 mS/cm (28 PSU). This discrepancy may be explained by the removal of data in January, a period when conductivity dropped to a minimum of 38 mS/cm (24 PSU) in VL2.

The boxplots indicate that the **pH fluctuations** in the seawater (Figure 12) are minimal. The maximum variation is only 0.2 and 0.3 for VL2 and VL1, respectively. The time series also show that the pH values are very stable with minimal fluctuations. At the beginning of the measurements, there is a slight downward trend until November, after which a gradual increase occurs until the end of the measurements. Throughout the measurement period, the pH values fluctuate around an average of 8.1 for VL2. For VL1 the time series also show slightly more variation in the measurements. This variation can possibly be attributed to the tidal action on VL1, which at certain times causes it to be submerged deeper in the water than VL2. Another explanation could be the formation of a biofilm around this pH sensor.

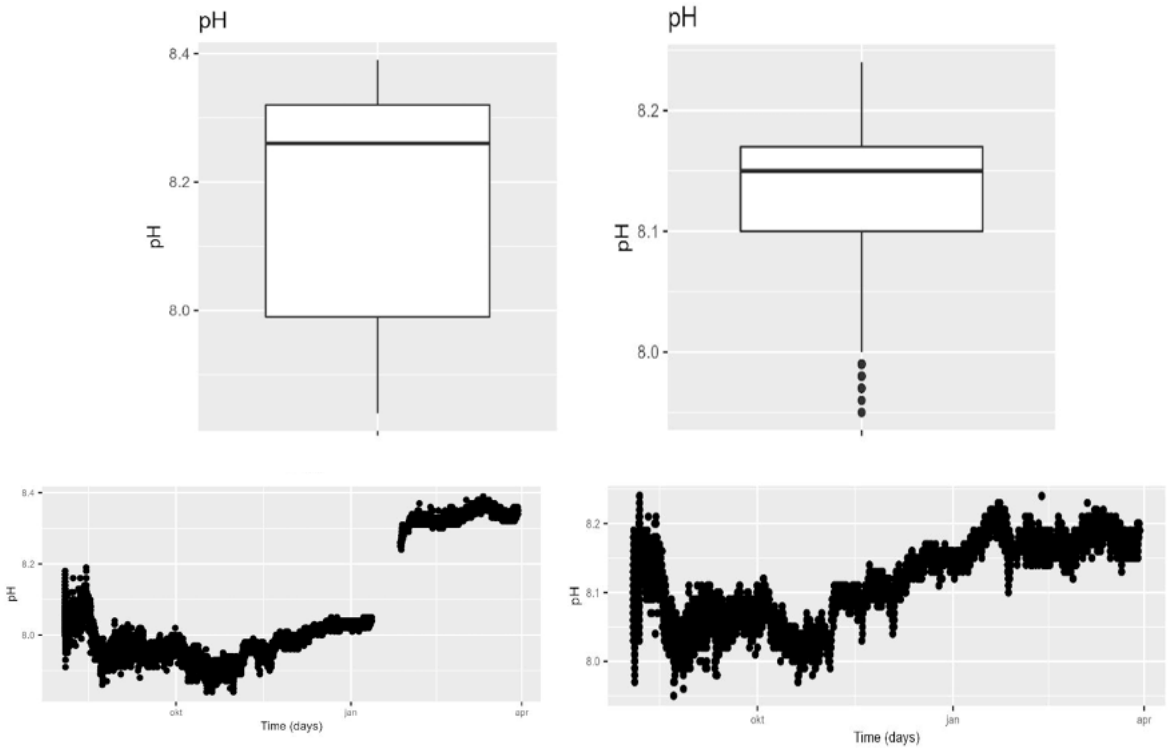

Figure 12. pH of the water in the port of Vlissingen
Left: VL1; right: VL2.

For VL2 there is a stepwise increase in the **oxidation-reduction potential (ORP)** until the end of January, after which it drops suddenly from 500 mV to 100 mV (Figure 13). The data from VL1 show a similar decrease. From February onwards, the redox potential appears to gradually increase again. For VL1 there is also a drop to 200 mV in November, for which there is also no explanation. Both boxplots show similar patterns. The median redox potential is in the range of 200 to 250 mV for both setups.

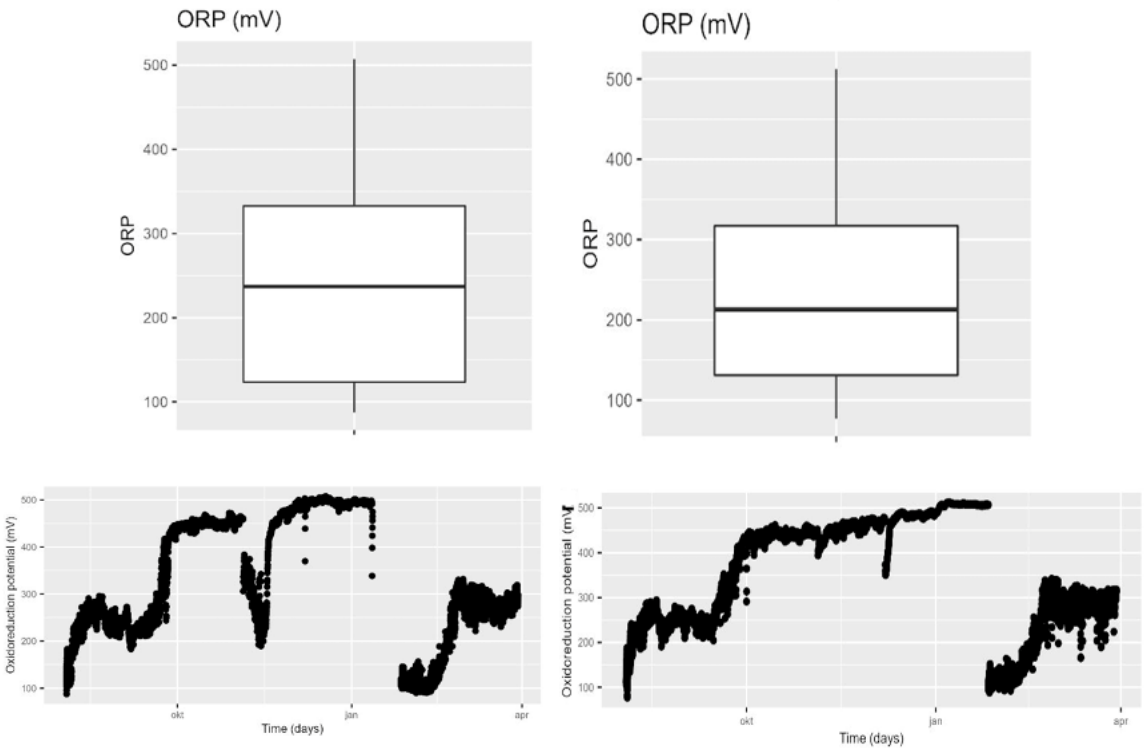

Figure 13. Redox potential of the water in the port of Vlissingen
Left: VL1; right: VL2.

Correlations between environmental parameters

In this analysis, the pairwise correlations between different parameters from both setups in Vlissingen are discussed together (VL1: Figure 14; VL2: Figure 15), unless clear differences are observed. However, it is important to reiterate that for VL1 some of the data has been filtered out over a period of approximately 20 days. This deletion may partly explain the slight differences between the two locations.

The scatter plot shows a strong inverse relationship between temperature and dissolved oxygen (Figure 1), which is confirmed by the correlation coefficients of -0.900 and -0.933.

Based on the stable pH values during the entire measurement period, it can be concluded that the pH is little or no influence from other environmental factors. The high correlation coefficients of -0.725 and -0.608 can be attributed to the use of a very narrow scale range for the pH values. This confirms that the correlation between pH and other environmental factors is not significant.

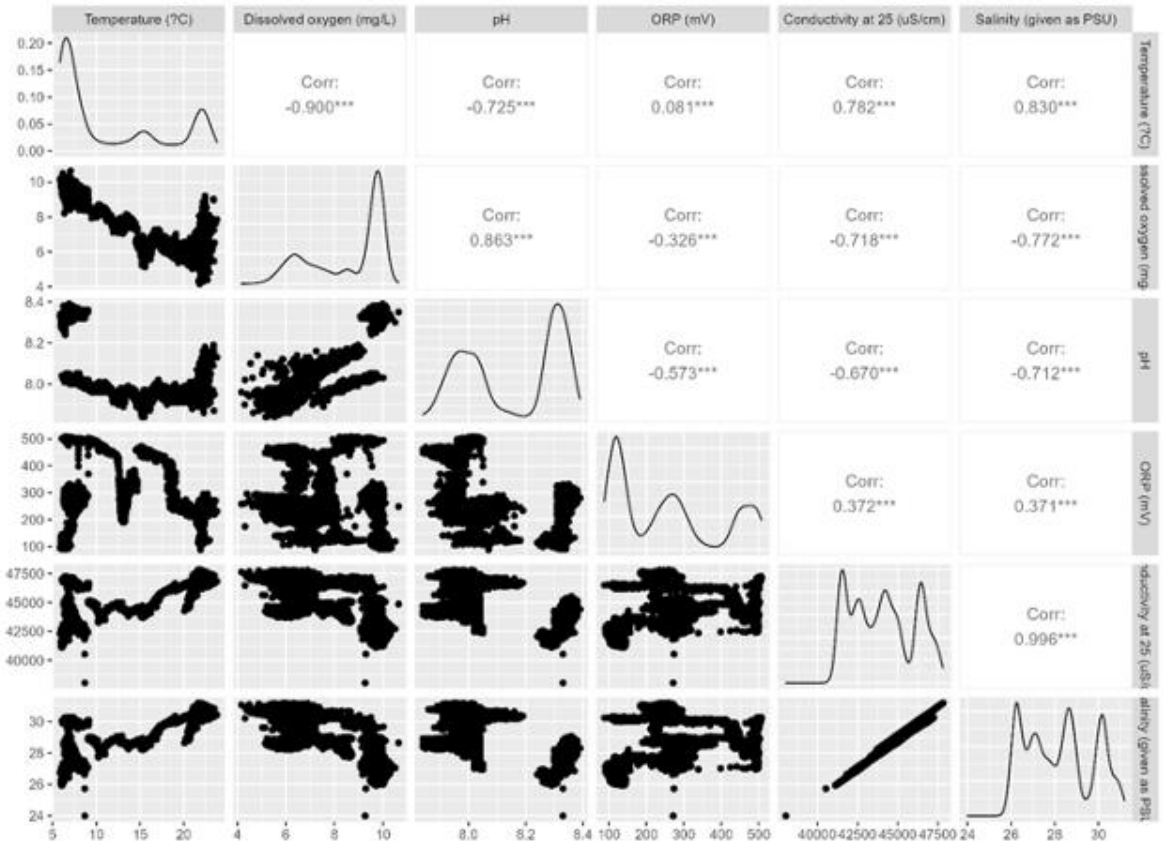

Figure 14. Correlation between the different environmental parameters in Vlissingen 1

There is no correlation between temperature and redox potential, with correlation coefficients of -0.081 and -0.074 for VL1 and VL2, respectively (Figure 14, Figure 15). Literature confirms that there is no direct relationship between the two variables. However, this does not mean that there cannot be an indirect relationship between temperature and redox potential.

The main difference between the correlation analyses in Vlissingen and the neighbouring demonstrator in Ostend can be found in the scatter plots of temperature in combination with specific conductivity and salinity. This is because the water in Vlissingen has much more stable values for conductivity and salinity. In Vlissingen a correlation is found between temperature and conductivity of 0.782 and 0.692 for VL1 and VL2 respectively. A correlation of 0.830 and 0.763 respectively is also found for salinity and temperature. These findings suggest that there is a direct proportional relationship between temperature and salinity, with lower temperature associated with lower salinity. This is confirmed by the observations of the time series (Figure 11), where the salinity is lower in the winter months. In the summer months, the water evaporates more due to the higher temperatures, resulting in a relatively higher salinity.

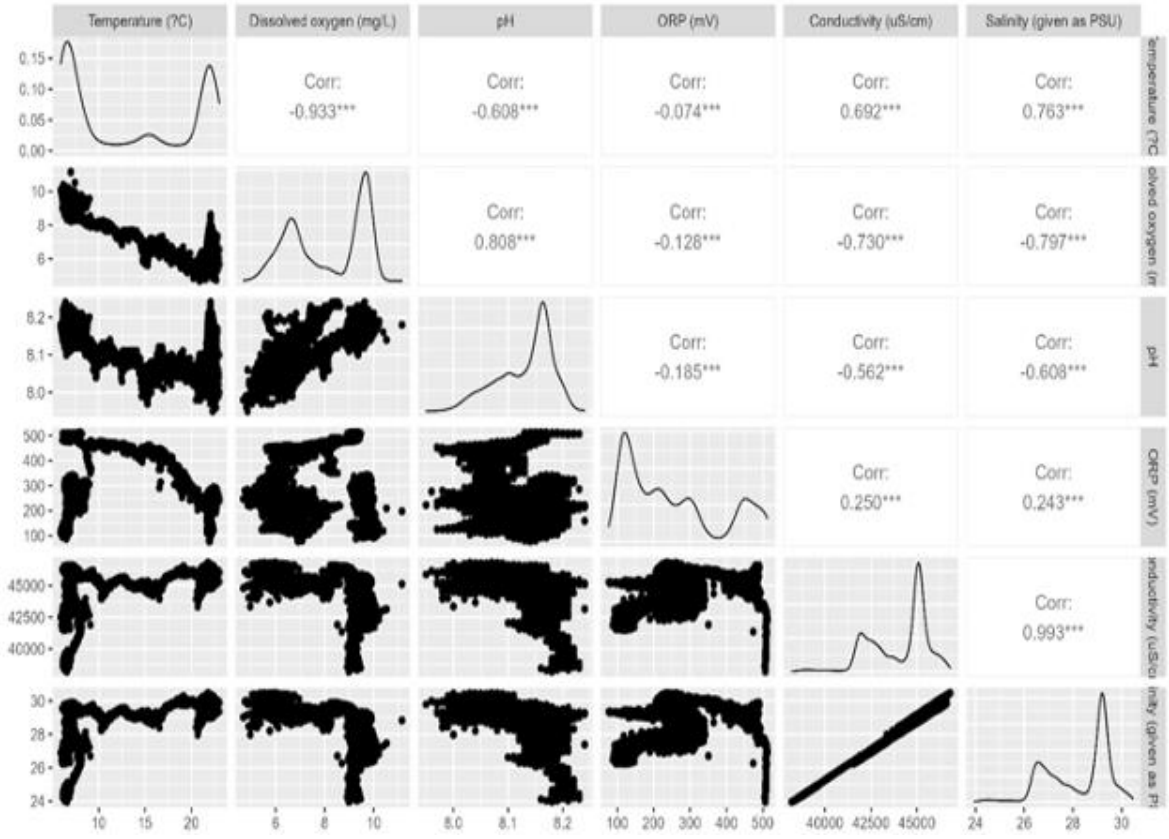

Figure 15. Correlation between the different environmental parameters in Vlissingen 2

Subsequently, there is also a significant correlation between dissolved oxygen and specific conductivity, as well as between dissolved oxygen and salinity. For VL1 and VL2, the correlation coefficients are -0.718 and -0.730 for dissolved oxygen with specific conductivity, and -0.772 and -0.797 for dissolved oxygen with salinity, respectively. These correlations show a clear inverse relationship. This makes sense given the relationship between temperature and conductivity/salinity, and the inverse relationship between temperature and dissolved oxygen. In general, this means that as the amount of dissolved oxygen in seawater increases, the

salinity of the seawater decreases. Conversely, when the dissolved oxygen in seawater decreases, the salinity increases.

Principal component analysis

Another way to look at correlation is by a Principal Component Analysis (PCA). A PCA reduces the dimensionality of large datasets by converting a large set of variables (environmental parameters rate) to a smaller set (principal components) that still contains the most important information. To decide how many components should be studied, screeplots were created for Vlissingen 1 (Figure 16) and Vlissingen 2 (Figure 17). It is clear that the two first principal components (PC1 and PC2) can explain already 90% of the total variance seen in the original dataset for VL1, and 86% for VL2.

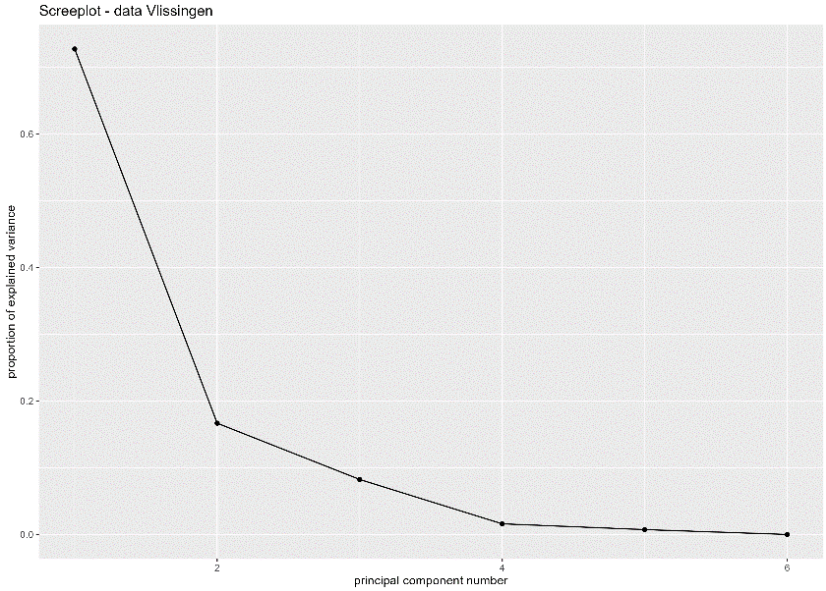

Figure 16. Scree plot for the PCA analysis of the environmental parameters at the VL1 demonstrator

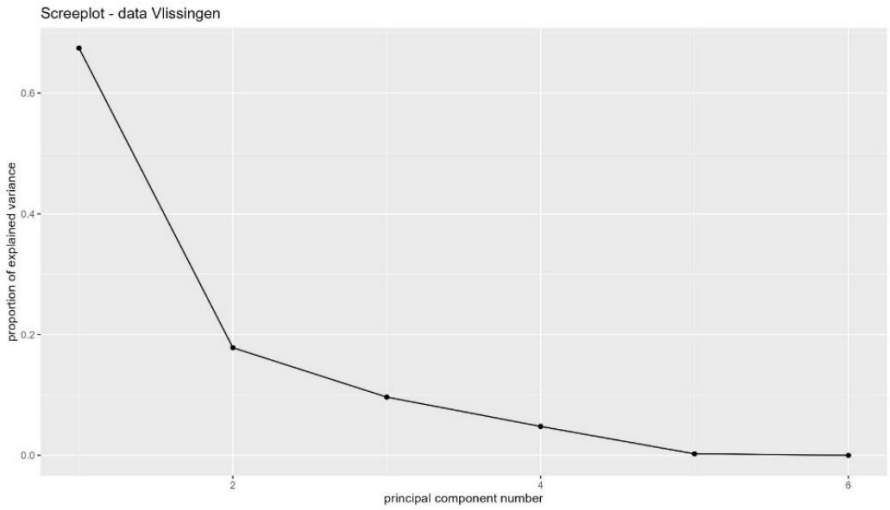

Figure 17. Scree plot for the PCA analysis of the environmental parameters at the VL2 demonstrator

The results of the PCA in Vlissingen confirm the inverse relationship between temperature and dissolved oxygen (Figure 18). In contrast to the PCA in Ostend, the PCA in Vlissingen clearly indicates that there is no direct relationship between the redox potential and the other environmental factors. Furthermore, in Vlissingen, again in contrast to in Ostend there is a slight correlation between the pH and the other environmental factors (except ORP). This can possibly be attributed to a misinterpretation of the scale of the pH graph. Although this graph shows a trend very similar to that of dissolved oxygen, a wider scale would show that pH values remain nearly constant and the graph nearly horizontal is.

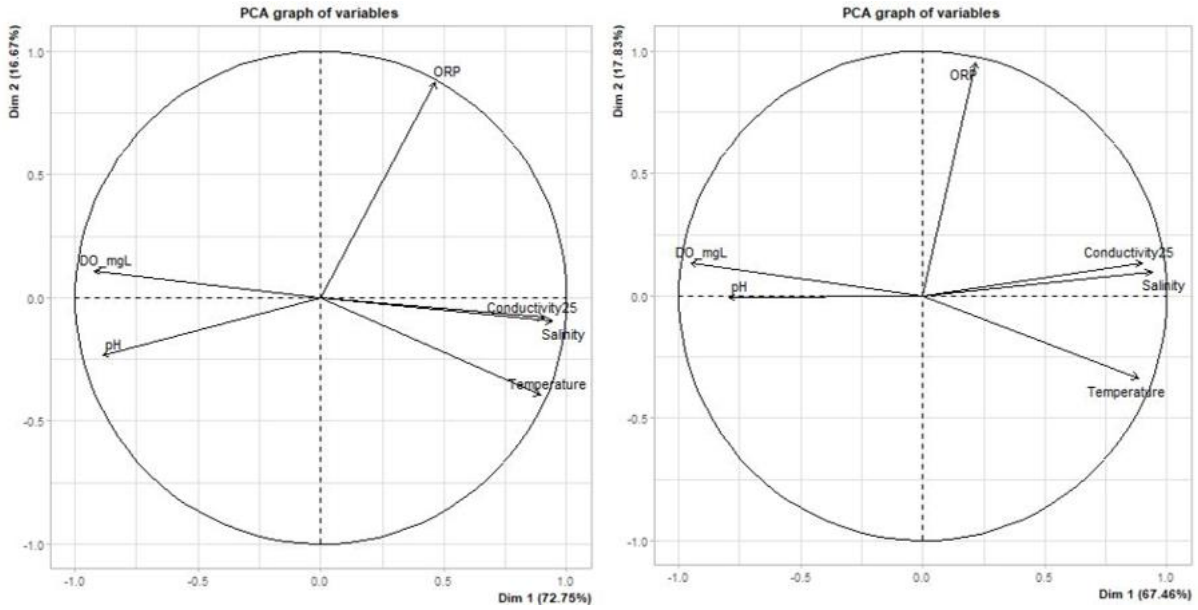

Figure 18. PCA biplot for the environmental data of the demonstrators at Vlissingen 1 (left) and Vlissingen 2 (right).

The PCA also confirms the findings of the correlation analysis regarding the relationship between conductivity/salinity on the one hand and temperature/dissolved oxygen on the other. A slightly positive correlation is observed between temperature and conductivity/salinity, while a slightly negative correlation is observed between dissolved oxygen and conductivity/salinity.

Corrosion measurements: experimental methodology

Steel types

Three specific steel types were selected for conducting the experiments: S235, S355 and 316L. In the following paragraphs, these individual steel types will be briefly described, explaining their characteristics and composition.

The first material is **S355 carbon steel**, which meets the European EN 10025:2 standard. This is a structural steel type (indicated by the "S" in the designation, which refers to "structural"). The value "355" stands for the minimum tensile strength of the material (355 MPa, for a sheet thickness of 16 mm). S355 can be classified as "mild steel" because of its relatively low carbon content, which makes it more suitable for welding work (de Jesus et al., 2012). The chemical and mechanical properties of the steel can be compared to those of the American standard variant ASTM A572/A709 (Igwemezie, Mehmanparast, & Kolios, 2018). S355 is widely used in various construction applications, including shipbuilding, bridge components, offshore structures and wind towers (Igwemezie et al., 2018).

S235 carbon steel follows the guidelines of the European Committee for Iron and Steel Standardization (ECISS), with a minimum tensile strength that is slightly lower than that of S355 for an equal thickness.

Both aforementioned structural steels belong to the category of low-carbon steels. The carbon limit for this category has been set at 0.30%, with both S235 with a maximum value of 0.22% C and S355 with a maximum value of 0.23% C more than comply. In addition to the carbon content, the American Iron and Steel Institute (AISI) also looks at the alloying elements in the steel. Since both S235 and S355 have a manganese content of up to 1.60%, they are classified as "plain carbon steel" (Singh, 2020). These classifications and limit values provide insight into the composition and properties of the steels. It is important to note that these low carbon steels will not perform optimally in terms of corrosion resistance. The material does not contain the crucial elements such as copper, chromium or nickel, which are of great importance for corrosion resistance. In the past, this material was available in a pickled and oiled form, which offered some degree of corrosion resistance.

Alloy 316L is a stainless steel with an austenitic structure containing chromium, nickel and molybdenum. The molybdenum improves corrosion resistance and resistance to pitting corrosion caused by chloride ion solutions, which often occur in water. In addition, it also increases strength at high temperatures. To provide protection against corrosion, a thin layer of metal oxides is applied to the surface, which acts as a barrier against corrosive substances. Typically, alloy 316L contains approximately 2-3% molybdenum, 16-18% chromium, 10%-14% nickel, 16-18% chromium, and 0.08% carbon. Other elements can be added to this alloy to modify the properties of the steel. Alloy 316L is widely used in marine equipment, refineries and chemical plants because of its excellent corrosion resistance, especially in highly corrosive environments.

Use of coupons for corrosion measurements

To completely submerge the metal coupons in water, racks were used to which the coupons were attached. To enable this attachment, two 8 mm diameter holes were drilled into the coupons. These holes were then used to securely fasten the coupons to the rack using tie wraps. Color coded tags were used to ensure that the different coupons could be identified throughout the study. These tags were attached individually to each plate, as well as to the rack itself. This made it possible to keep an overview of which coupons were still in the water and which had already been removed from the water. These identification tags were essential to enable proper tracking and analysis of the coupons throughout the research process.

The racks themselves were constructed using cut wire panels (Figure 19). This created a rectangular rack consisting of a grid of 3 by 9 compartments, resulting in a total of 27 coupons that could be attached to the rack. The racks themselves were also tagged, which were linked to specific locations. These tags were of a different color so that locations where the racks were used could be identified later. This tagging method was instrumental in maintaining traceability and facilitating the accurate identification of both coupons and racks throughout the research process.

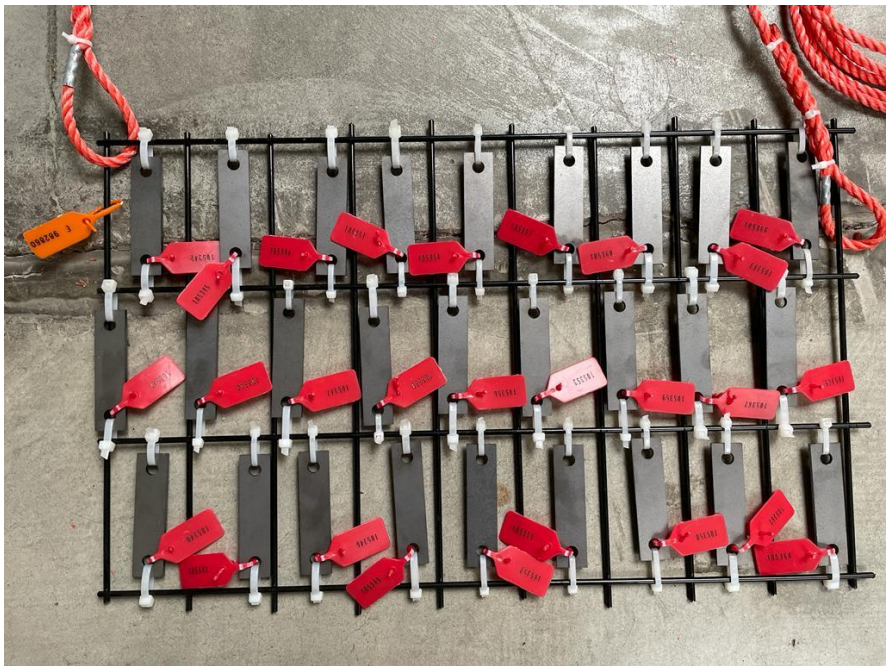

Figure 19. Rack of S355 coupons to be exposed to the seawater in Ostend

The racks were attached by means of an eye splice made of three-strand twisted polypropylene rope, whereby the corners of the rack were attached to this rope. To keep the rope from fraying, tie wraps and duct tape were used to hold the ends of the rope together (Figure 19).This specific construction method and fasteners ensured a firm and reliable suspension of the racks, allowing the coupons to be attached and submerged in the aquatic environment in a stable and consistent manner during the study.

On September 12, 2022, three racks were installed on the platform. The racks were carefully submerged at a depth of exactly 1 meter below the surface of the water. An eye splice was applied to the ends of the rope, allowing them to be hung from iron hooks on the platforms. During the installation of the racks, sufficient distance was also kept between the sensors and the racks to prevent any influence on the sensors.

Procedure for coupon measurements

Samples were collected at two, three and six months after the start of the exposure period. Whenever samples were taken, the rack was first taken out of the water to obtain a full picture of the rack. Subsequently, four samples per rack were taken.

Three coupons were thoroughly cleaned with water, dried with paper towels, wrapped in paper towels and placed in a sealed freezer bag with silica gel to prevent further corrosion. One coupon was not cleaned and was placed in a freezer bag without touching it. The purpose of this action was to perform a visual inspection on the coupon in the future. The date and location of sampling were documented on the pouch, after which the pouch was carefully sealed. Rack was then replaced under water.

The coupons were cleaned in accordance with the guidelines set forth in the ASTM G1 standard. After cleaning, the weight loss and corrosion rate of the coupons were evaluated to understand their corrosion behaviour. Measuring the weight loss and corrosion rate provides valuable information about the interaction between the coupon material and the environment in which they are exposed and can serve as an indicator of the durability and performance of the material in corrosive conditions. To determine the corrosion rate based on the mass loss, the corrosion products were first removed from the coupons. For this purpose, the metal coupons were placed in 200 ml 23% hydrochloric acid in glass beakers for 15 minutes. After the acid treatment, the coupons were thoroughly rinsed with demineralized water and dried with paper. To ensure the accuracy of the measurement, it was ensured that the coupons were completely dry before being weighed. At the start and after the cleaning process, the coupons were photographed with the corresponding tags.

At the start of the exposure, 30 coupons, per steel grade, were used to determine the average initial masses. Subsequently, at different times (approximately 2, 3 and 6 months after exposure to seawater), four coupons were collected from each steel grade, three of which were for mass loss measurements. For the determination of the corrosion rate, the mass change of the coupons was measured and extrapolated to a corrosion rate.

Use of the CCube LP sensor

For the SOCORRO project, bespoke sensor systems been developed for corrosion measurement CCube (Delft, the Netherlands). The sensor is based on linear polarization resistance (LP) theory to measure the rate of corrosion. This is achieved by applying small voltages (less than ±30 mV) to the metal just above and below the corrosion potential. Within this voltage range, the resulting current response is linear if the anodic and cathodic regions are equal (Campos-Silva & Rodríguez-Castro, 2015; Ropital, 2011). This makes it possible to determine the polarization resistance (Rp), which is defined as the slope of the current-potential curve according to the Stern-Geary equation (Stern & Geaby, 1957):

$$I_{Corr} = \frac{1}{R_p} * \frac{\beta_a * \beta_c}{2.303(\beta_a * \beta_c)}$$

with

$$B = \frac{\beta_a * \beta_c}{2.303(\beta_a * \beta_c)}$$

B is a constant that depends on the anodic and cathodic table diagram (β_a and β_c) obtained from polarization curves. In most cases, the values of β are between 60 and 120 mV (García-Galvan, Fajardo, Barranco, & Feliu, 2021).

$$I_{Corr} = \frac{B}{R_p}$$

Faraday's law can then be applied to calculate the corrosion rate as follows:

$$CR = K_1 * \frac{I_{Corr}}{dA} * EW$$

whereby CR = corrosion rate in mm/year, K_1 = constant of $3.27*10^{-3}$, d = density in g/cm³, EW = the equivalent weight, defined as the mass in grams oxidized by the passage of an electrical charge of 1 Faraday. EW values can be found for different metals in ASTM G102 (García-Galvan et al., 2021).

The CCube uses working electrodes made from the three different steel grades in the project (S355, 316L and S235) and a micro-electrochemical cell that measures the rate of corrosion. These measurements are performed every four hours. The working and reference electrodes are housed in a plastic housing filled with epoxy adhesive for protection against sea water, with dimensions of 150 mm (length) x 60 mm (height) x 50 mm (width).

The sensor is connected to a separate CCube control box located in an easily accessible position. A potentiostat and a data logger are installed in the control cabinet. In addition, the control box contains a mobile antenna that transmits the measured data to the CCube network. The company collects all sensor data and sends it to an online database that is accessible to all researchers of the SOCORRO project.

On 3 August 2022, the CCube probes were installed in the water for the first time, together with the environmental sensors. Due to cabling errors at the company, which only became clear after several months, all data generated by the CCube LP probe until March 1, 2023, were unusable. Afterwards, the cabling in the probes was correctly reconnected, so that the sensors have been functioning properly. However, when interpreting the CCube data, it must be considered that the sensors were not new when placed in the water and already showed some traces of corrosion. Some sensors showed more corrosion than others (Figure 20).

Figure 20. CCube probes at VL1 (left) and VL2 (right) before re-installation

Corrosion: results

Corrosion rates obtained through coupon measurements

The following graphs present the results of the mass loss measurement on the steel coupons, with the measurements converted to corrosion rate. The corrosion rate was measured for three different time periods of two, three and six months respectively for each set-up.

For **S355 low carbon steel** (Figure 21A) the corrosion rate is highest between months two and three, followed by a decrease in corrosion rate over time. The initial high corrosion rate, namely 0.400 ± 0.016 mm/year for VL1, 0.285 ± 0.016 mm/year for VL2 and 0.301 ± 0.003 mm/year, can be attributed to the formation of corrosion products that spread throughout the initial stage of uniform corrosion entire surface. Once formed, these corrosion products act as a passivation layer, resulting in a reduction in the corrosion rate.

A similar trend can also be observed for **S235** (Figure 21B), where a high initial corrosion rate is first observed, followed by a decrease in corrosion rate. Much variation can be seen in the corrosion rate of VL2 in the 2nd month, namely a standard error of 0.044 mm/year, compared to a standard error of 0.025 mm/year for VL1.

For the **316L steel** (Figure 11) it can be seen that the corrosion rate is practically zero during the measurement period of 6 months. These findings highlight the exceptional corrosion resistance of 316L steel, particularly in the seawater environment. The steel retains its integrity and shows virtually no signs of corrosion during the six-month study period. This is consistent with the known properties of 316L steel.

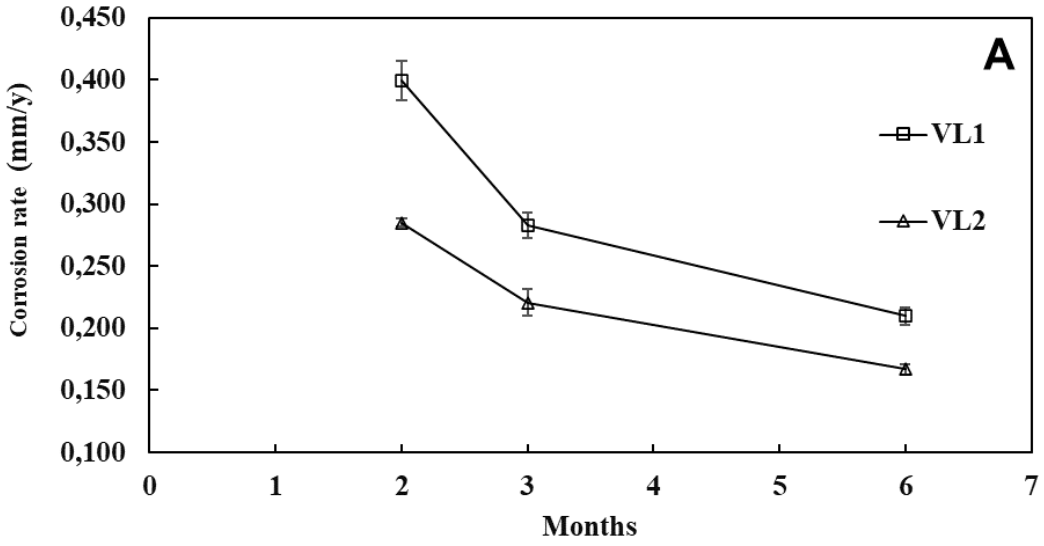
A
VL1
VL2
Corrosion rate (mm/y)
0,450
0,400
0,350
0,300
0,250
0,200
0,150
0,100
0
1
2
3
4
5
6
7
Months

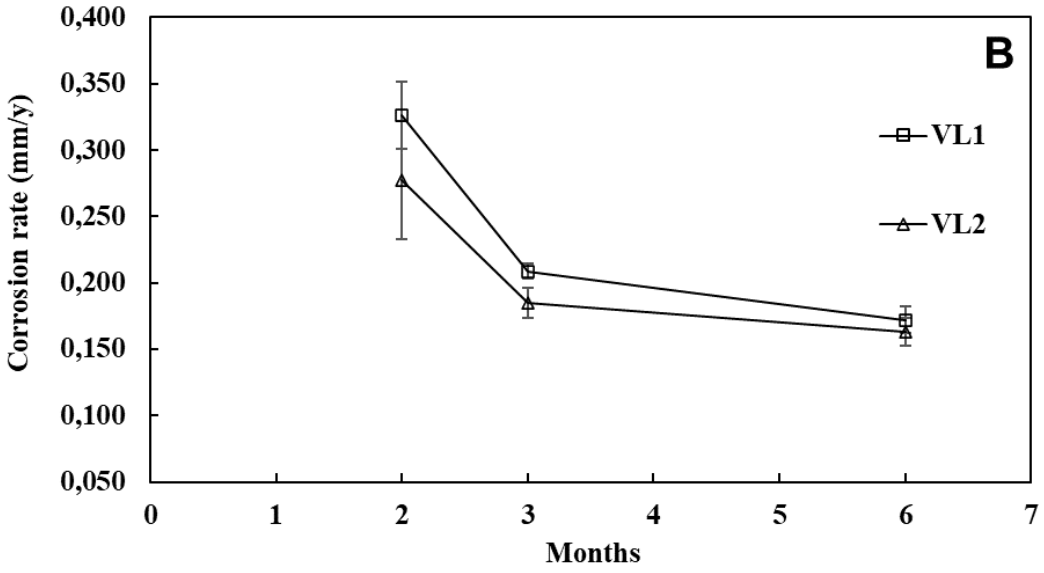
B
VL1
VL2
Corrosion rate (mm/y)
0,400
0,350
0,300
0,250
0,200
0,150
0,100
0,050
0
1
2
3
4
5
6
7
Months

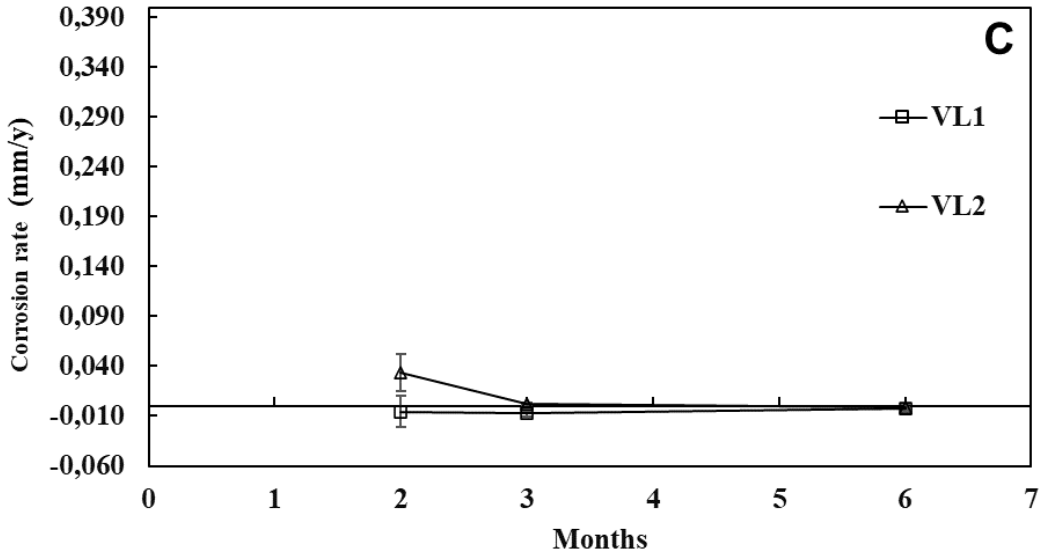
C
VL1
VL2
Corrosion rate (mm/y)
0,390
0,340
0,290
0,240
0,190
0,140
0,090
0,040
-0,010
-0,060
0
1
2
3
4
5
6
7
Months

Figure 21. Corrosion rates of (A) S355, (B) S235 and (C) 316L steel coupons at the Vlissingen demonstrators

Corrosion rates obtained through LP measurements

For VL1, the CCube data (Figure 22, top) show a corrosion rate for **low carbon steel S355** between 0.550 mm/year and 0.875 mm/year. From the mass loss measurements in paragraph 0 it is deduced that the corrosion rate on 01/03/2023 was 0.210 mm/year. This decrease in corrosion rate is expected because the sensor was not cleaned on 01/03/2023. Part of the data around the second week of May for the CCube measurements are also missing.

The CCube data for VL2 (Figure 22, bottom) describe a corrosion rate between 0.950 mm/year and 1.450 mm/year. The mass loss measurements in paragraph 0 show that the corrosion rate on 01/03/2023 was 0.166 mm/year. However, a small increase is expected in these measurements, as VL2's CCube sensor was cleaned on 01/03/2023. The expected small increase in the corrosion rate is attributed to this sensor being re-exposed to "initial" corrosion. However, the observed increase is significantly higher than expected as a corrosion rate of 0.285 mm/year was measured after two months of immersion. This still implies a difference of about 1 mm/year with the CCube sensor, which was immersed for an equal period of time (between 01/03/2023 and 25/04/2023).

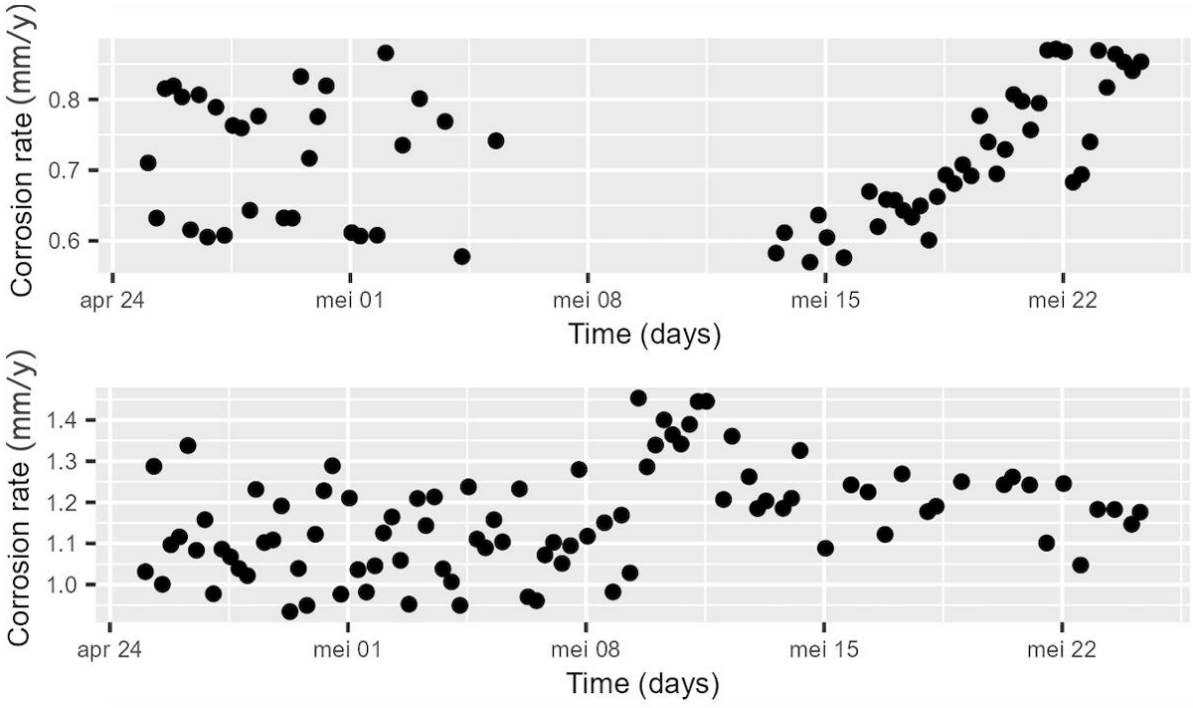

Figure 22. LP corrosion rate measurements for S355 low carbon steel at the Vlissingen demonstration. Top: VL1; bottom: VL2.

First of all, it is noticeable that the data for S235 (Figure 23) show a much lower spread than the obtained data for S355 (Figure 22), so that a clearer pattern is visible. The results for VL1 (Figure 23, top) show a decreasing trend from about 0.460 mm/year to 0.425 mm/year,

followed by an increase to 0.480 mm/year. For VL2 the results fluctuate between 0.850 and 1.000 mm/year (Figure 23, bottom) Since the sensor for this setup has been cleaned, the corrosion rate is expected to be slightly higher than the corrosion rate measured on 01/ 03/2023 by the mass loss measurement (0.163 mm/year). Still, the difference is too high to be statistically in the same range. Hence, the CCube results and the measurements on the sample coupons are contradictory.

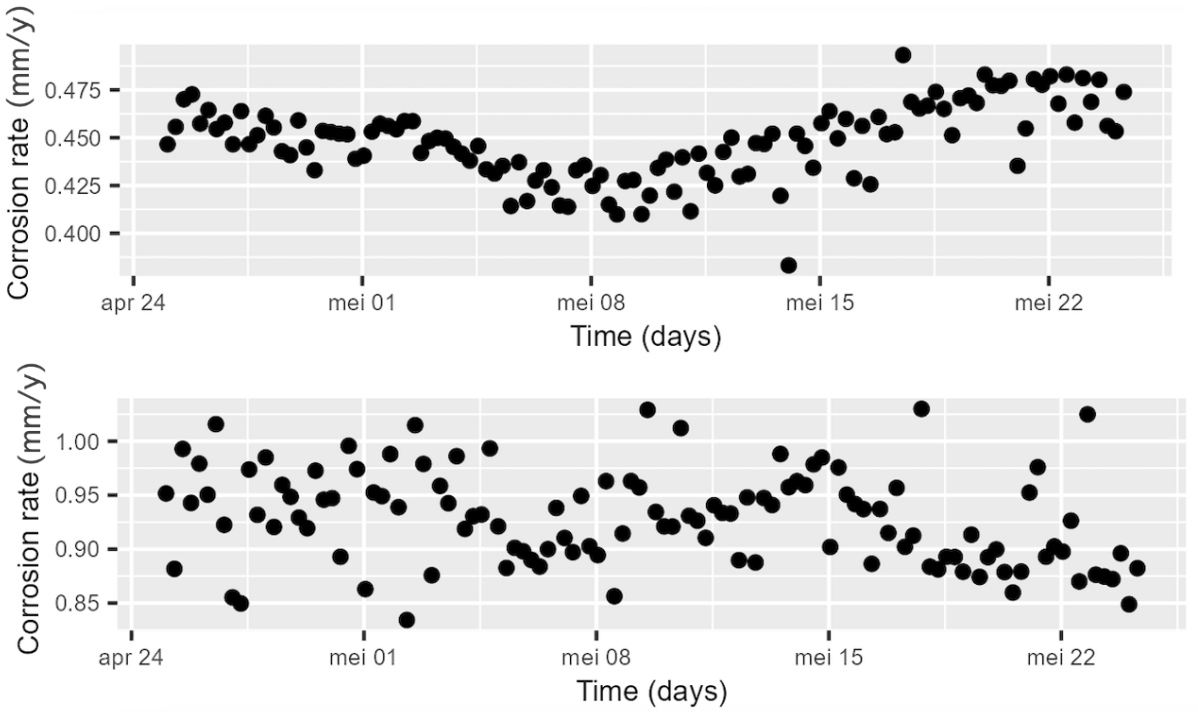

Figure 23. LP corrosion rate measurements for S235 low carbon steel at the Vlissingen demonstration. Top: VL1; bottom: VL2.

The CCube sensors show that the corrosion rate of 316L steel is practically zero for this study (Figure 24). If presented on the same scale as for S355 and S235, the corrosion rate would be around zero. For reference, the highest measured corrosion rate for 316L by the CCube is 0.015 mm/year. This is even lower than the corrosion rate measured with the mass loss measurement, where the initial measurement resulted in 0.034 mm/year.

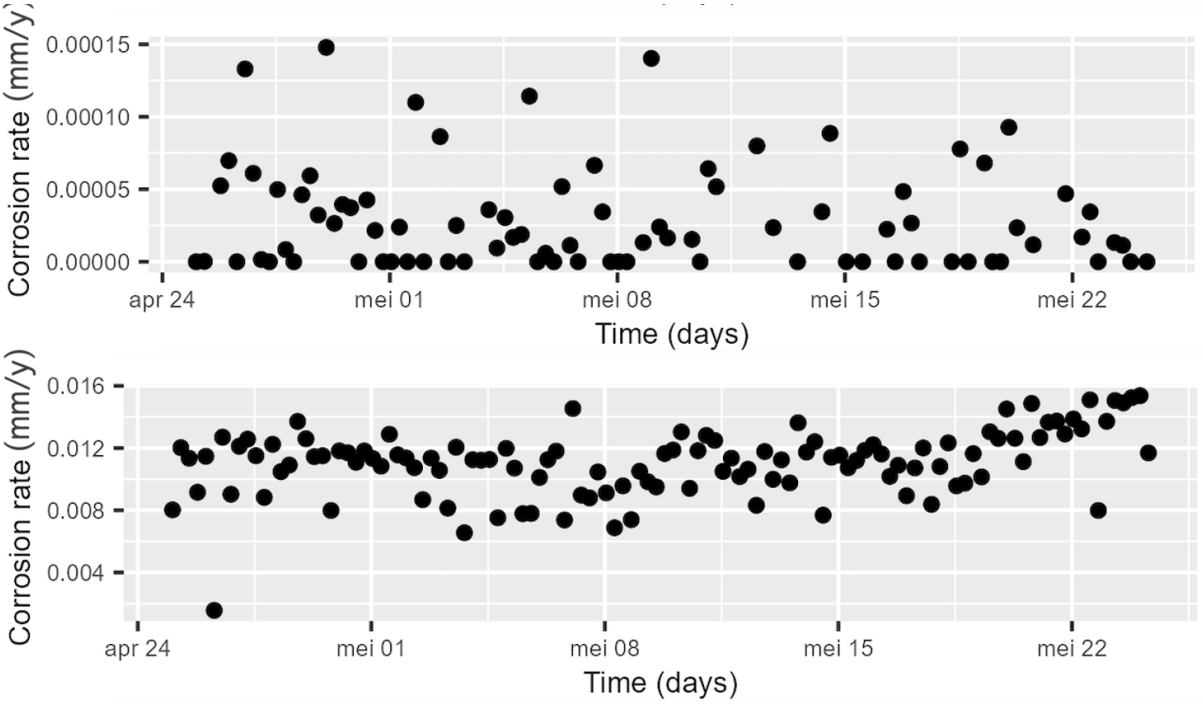

Figure 24. LP corrosion rate measurements for 316L stainless steel at the Vlissingen demonstration. Top: VL1; bottom: VL2.

Correlation between LP corrosion measurements and environmental parameters

PCA plots were created to investigate the correlations between the different environmental parameters with the corrosion data added to the dataset. Analyses were performed for S355 (Figure 25), S235 (Figure 26) and 316L steel (Figure 27).

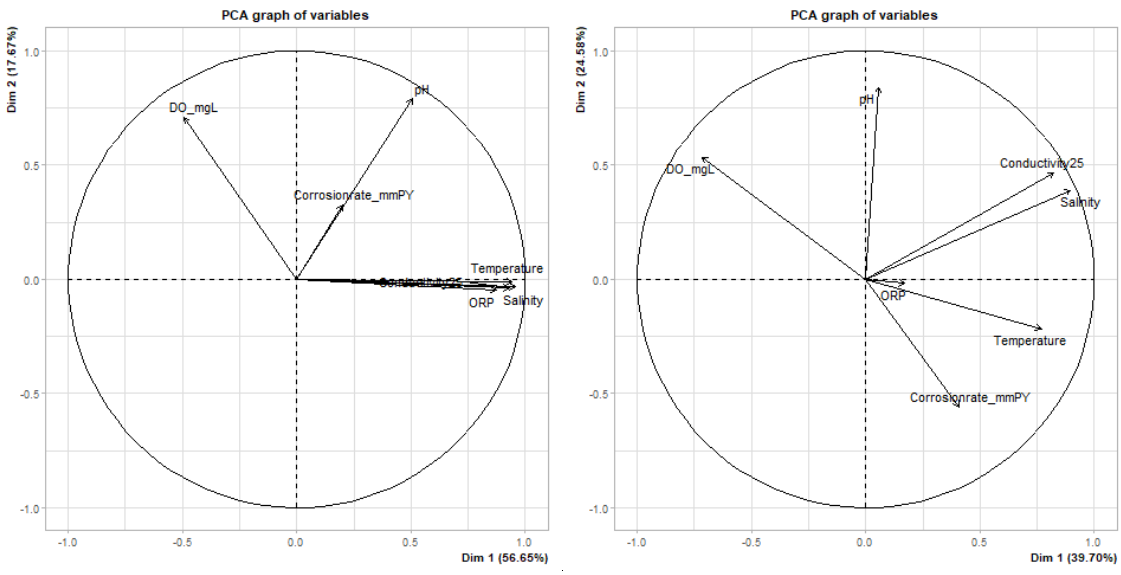

Figure 25. PCA plots for the corrosion of S355 at the demonstrators in Vlissingen.

Left: VL1; right: VL2.

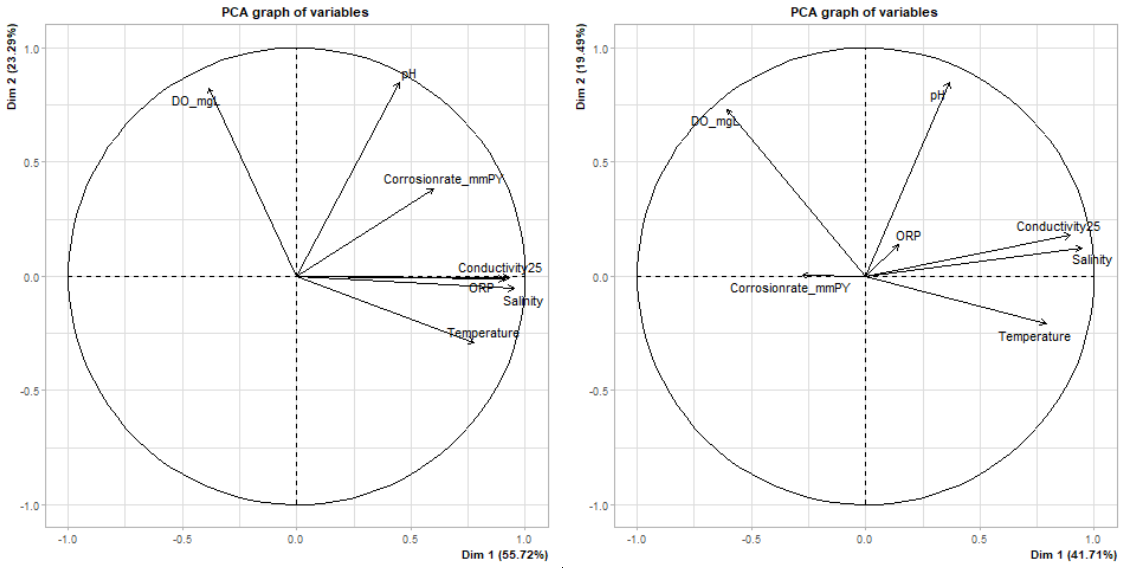

Figure 26. PCA plots for the corrosion of S235 at the demonstrators in Vlissingen. Left: VL1; right: VL2.

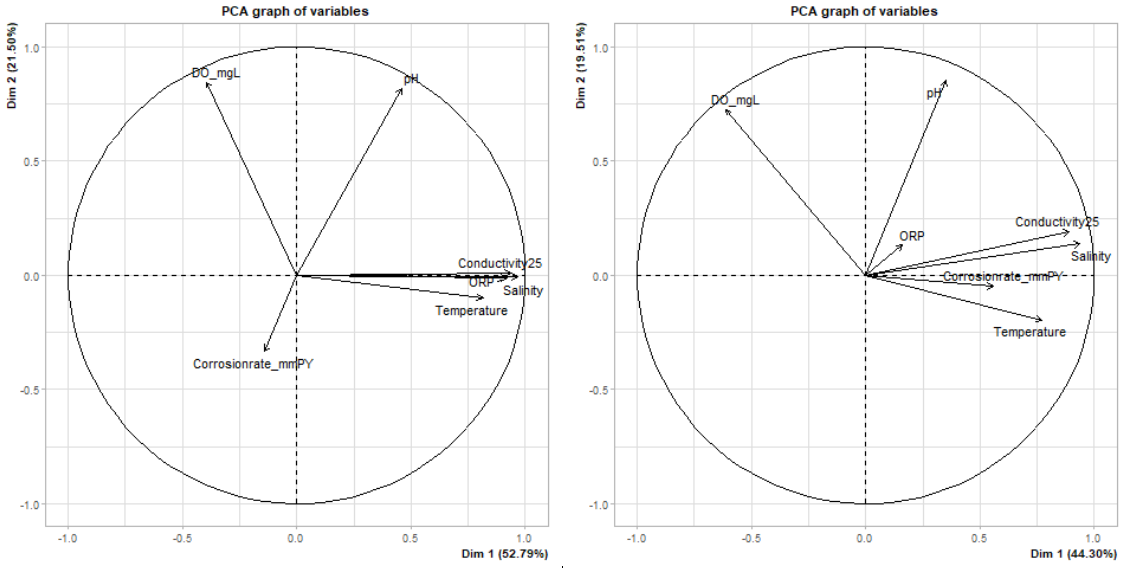

Figure 27. PCA plots for the corrosion of 316L at the demonstrators in Vlissingen. Left: VL1; right: VL2.

Use of the SOCORRO approach

In order to test the SOCORRO algorithm, environmental parameters sere uploaded in the SOCORRO app (https://app-c14q.onrender.com/) and the outcome (corrosion rate in mm/year) was compared with the corrosion rate of the coupons (initial value).

The corrosion rate (measured after three months of the experiment) fits very well with the predicted rate by the SOCORRO algorithm. As time goes by, the predicted corrosion rate changes along with (mostly) temperature, but moves away from the physical corrosion data from both coupons and LP measurements. This suggests that there is a time factor which is still not correctly captured by the model, and which, in practice, is related to the formation of a corrosion product layer on top of the coupons as well as the LP sensors. This time-dependent decrease should be incorporated into the next versions of the algorithm.

Table 2. Comparison of corrosion rates for coupons, LP measurements and the SOCORRO algorithm. Corrosion rates are expressed in mm/year. Standard error given for coupon data (n = 3)

VLISSINGEN 1	2 months	3 months	4 months	6 months
Coupons	0.33 ± 0.04	0.209 ± 0.008		0.172 ± 0.014
CCube			0.45	
Algorithm			0.21-0.23	
VLISSINGEN 2			**4 months**	
Coupons	0.28 ± 0.06	0.185 ± 0.016		0.163 ± 0.015
CCube			0.85 – 1.00	
Algorithm			0.195-0.21	

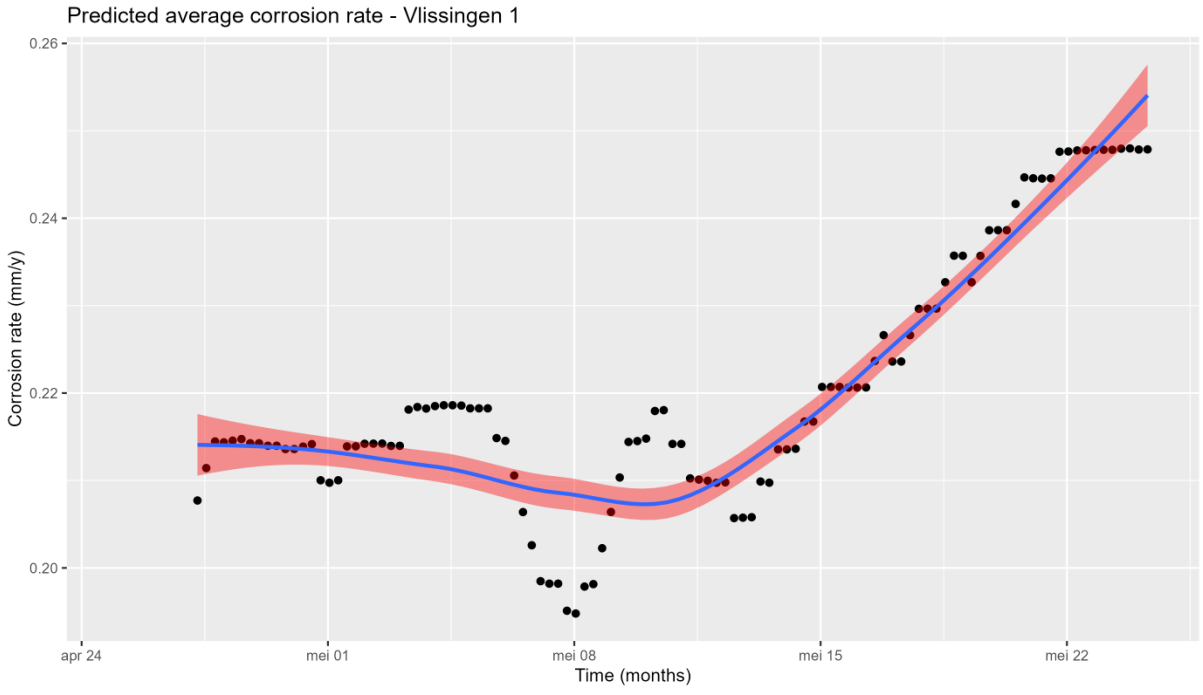

Figure 28. Predicted corrosion rate for S235 at Vlissingen 1 by the SOCORRO algorithm.
Bottom: predicted corrosion rates for every time point based on local averages of the different environmental points in May 2023
Blue line gives a loess regression line for the dataset with a red 95% confidentiality zone.

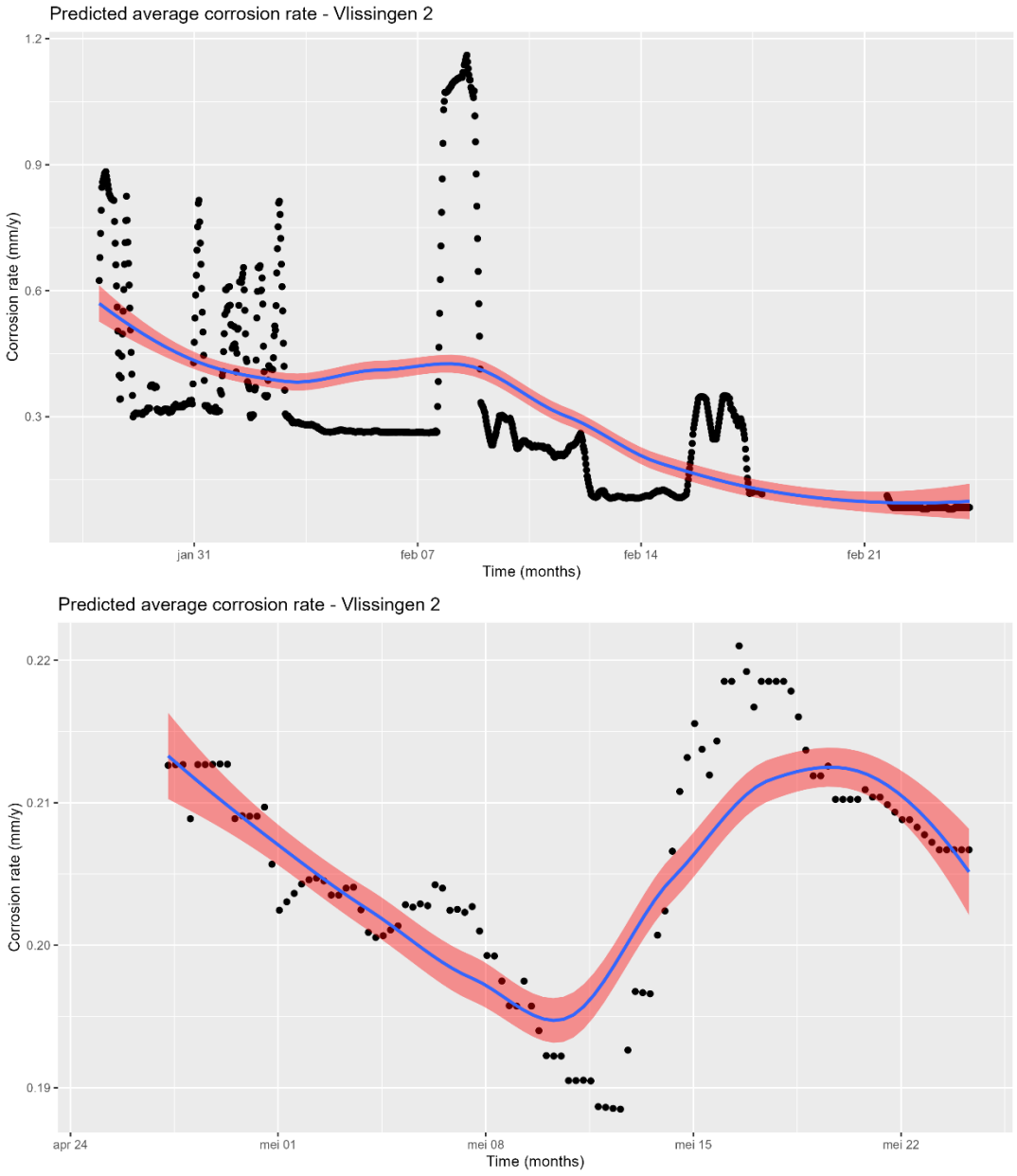

Figure 29. Predicted corrosion rate for S235 at Vlissingen 2 by the SOCORRO algorithm.
Top: predicted corrosion data for every time point based on local averages of the different environmental points between August 2022 and February 2023
Bottom: predicted corrosion rates for every time point based on local averages of the different environmental points in May 2023
Blue line gives a loess regression line for the dataset with a red 95% confidentiality zone.

Plans for further use?

The Vlissingen platforms will continue to serve as a Living lab, managed by Antwerp Maritime Academy, as a follow-up for Interreg 2 Seas SOCORRO and Interreg Vlaanderen-Nederland Praktijklab Corrosie en Isolatie. The data obtained in this Living lab will continue to serve as a baseline for other industrial tests. For example, a comparison will be set up to compare different corrosion protection mechanisms.

A copy of Vlissingen 2 may be placed (if the project application is approved) in the port of Antwerp as well.

The data collected will be fed into the algorithm to create a better model for marine installations, and to work out the incorporation of a time-delay effect.